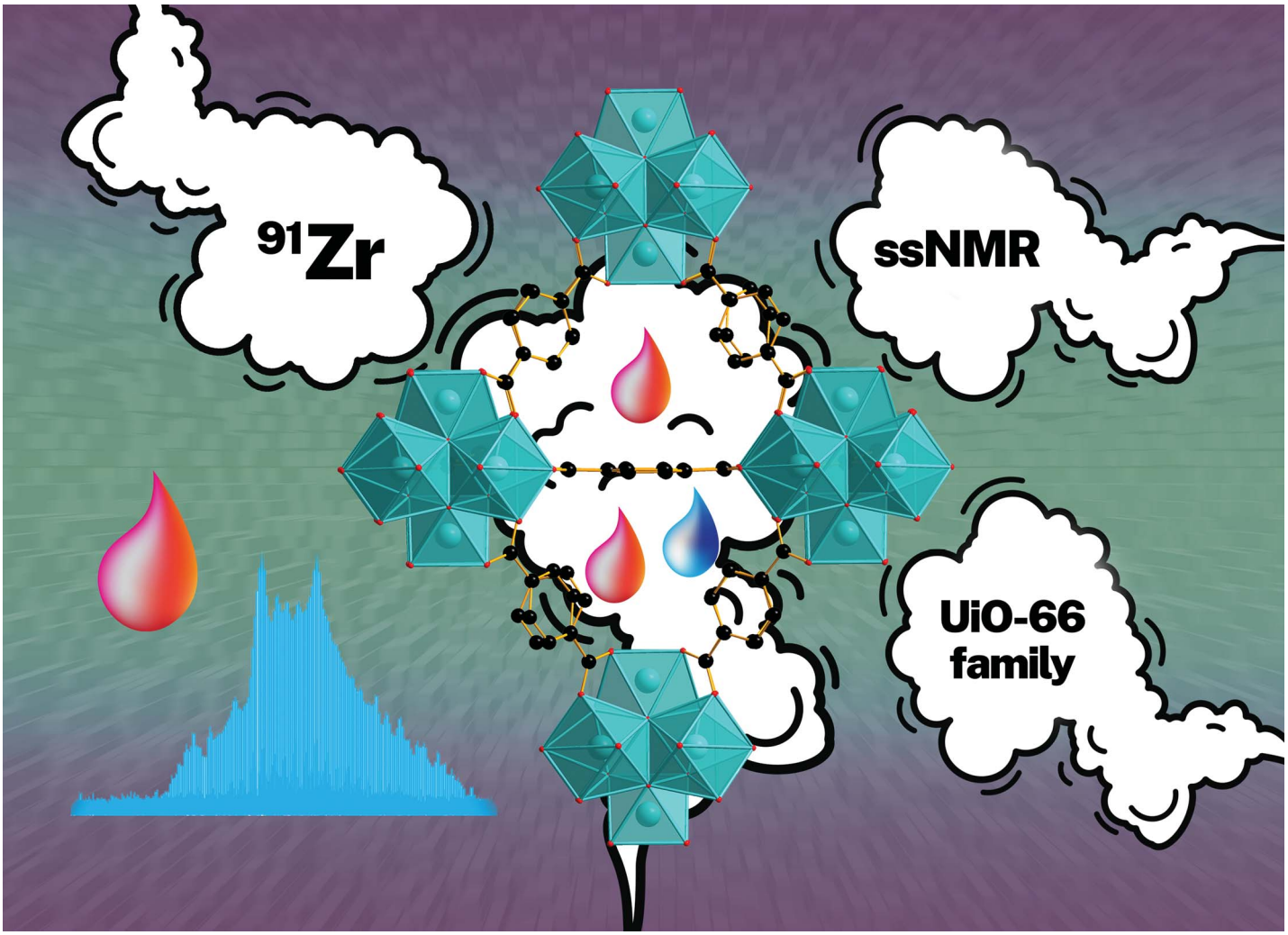

Showcasing research from Professor Pourpoint's laboratory, UCCS, Centrale Lille, Lille, France.

Probing the water adsorption and stability under steam flow of Zr-based metal–organic frameworks using ^{91}Zr solid-state NMR spectroscopy

We investigated the stability of three zirconium-based MOFs under steam flow at different temperatures using advanced ^{91}Zr solid-state NMR and DFT calculations.

As featured in:

See Frédérique Pourpoint *et al.*, *Chem. Sci.*, 2025, **16**, 69.

ROYAL SOCIETY OF CHEMISTRY

15 YEARS ANNIVERSARY

rsc.li/chemical-science

Registered charity number: 207890

Chemical Science

ROYAL SOCIETY OF CHEMISTRY

EDGE ARTICLE

View Article Online
View Journal | View Issue

Cite this: *Chem. Sci.*, 2025, **16**, 69

All publication charges for this article have been paid for by the Royal Society of Chemistry

Probing the water adsorption and stability under steam flow of Zr-based metal–organic frameworks using ^{91}Zr solid-state NMR spectroscopy†

Athulya Nadol, [a] Florian Venel,[a] Raynald Giovine,[a] Maëva Leloire, [a] Christophe Volkringer, [a] Thierry Loiseau, [a] Christel Gervais, [b] Caroline Mellot-Draznieks, [c] Bertrand Doumert,[d] Julien Trébosc, [d] Olivier Lafon [a] and Frédérique Pourpoint *[ae]

The stability of metal–organic frameworks (MOFs) in the presence of water is crucial for a wide range of applications, including the production of freshwater, desiccation, humidity control, heat pumps/chillers and capture and separation of gases. In particular, their stability under steam flow is essential since most industrial streams contain water vapor. Nevertheless, to the best of our knowledge, the stability under steam flow of Zr-based MOFs, which are among the most widely studied MOFs, has not been investigated so far. We explore it herein for three UiO-like Zr-based MOFs built from the same Zr cluster but distinct organic linkers at temperature ranging from 80 to 200 °C. We demonstrate the possibility of acquiring their ^{91}Zr NMR spectra using high magnetic field (18.8 T) and low temperature (140 K) and of interpreting them by comparing experimental data with NMR parameters calculated by DFT. NMR observation of this challenging isotope combined with more conventional techniques, such as N_2 adsorption, X-ray diffraction, IR, and ^{1}H and ^{13}C solid-state NMR spectroscopies, provides information not only on the possible collapse of the MOF framework but also on the adsorption of molecules into the pores. We notably show that UiO-66(Zr) and UiO-66-Fum(Zr) built from terephthalate and fumarate linkers, respectively, are stable over 24 h (and even over 7 days for UiO-66(Zr)) under steam flow at all investigated temperatures, whereas UiO-67-NH_2 containing a 2-amino-[1,1′-biphenyl]-4,4′-dicarboxylate linker degrades under steam flow at temperatures ranging from 80 to 150 °C but is preserved at 200 °C. The lower stability of UiO-67-NH_2 stems from its larger pores and its weaker Zr–O coordination bonds, whereas its preservation at 200 °C results from a more limited condensation of water in the pores.

Received 10th July 2024
Accepted 6th November 2024

DOI: 10.1039/d4sc04589k

rsc.li/chemical-science

1. Introduction

Although water covers 70% of the Earth's surface, less than 1% corresponds to accessible freshwater.[1] Furthermore, freshwater is unevenly distributed among countries and the United Nations estimates that 60% of the world's population lives in regions with nearly permanent water stress.[1] This number is expected to grow owing to climate change, increasing world population, improvement in living conditions and rise in water pollution. As a result, water scarcity is one of the greatest global risks.

In this context, metal–organic frameworks (MOFs) have recently attracted great interest for the production of freshwater since they can be used either to harvest water from the atmosphere[2,3] or to remove contaminants from wastewater.[4–7] Their high porosity results in large uptake capacity, whereas their high structural and chemical tunability allows their adsorption properties to be tailored. Adsorption of water in MOFs is also important for other emerging applications of these sorbents, including desiccation, humidity control, heat pumps/chillers and capture and separation of gases, such as CO_2.[8–10]

Consequently, it is essential to control the adsorption of water and the stability of the MOF in the presence of water in liquid and/or gaseous states.[9,11,12] In particular, it has been shown that Zr-based MOFs, such as UiO-66(Zr), benefit from a high stability in the presence of water.[6,9,13–16] This stems from the strength of Zr-carboxylate bonds and the high connectivity of Zr clusters. So far, the hydrothermal stability of these MOFs has been mainly investigated in liquid water, whereas the

[a]*Univ. Lille, CNRS, Centrale Lille, ENSCL, Univ. Artois, UMR 8181 – UCCS – Unité de Catalyse et Chimie du Solide, F-59000 Lille, France. E-mail: frederique.pourpoint@centralelille.fr*

[b]*LCMCP, UMR 7574, Sorbonne Université, CNRS, F-75005 Paris, France*

[c]*Laboratoire de Chimie des Processus Biologiques (LCPB), CNRS UMR 8229, Collège de France, PSL University, Sorbonne Université, Paris 75231, France*

[d]*IMEC, Univ. Lille, CNRS, Centrale Lille, Univ. Artois, FR 2638, F-59000 Lille, France*

[e]*Institut Universitaire de France, 1, rue Descartes, 75231 Paris CEDEX 05, France*

† Electronic supplementary information (ESI) available. See DOI: https://doi.org/10.1039/d4sc04589k

studies in the presence of water vapors are more limited.[14] To the best of our knowledge, no study under steam flow has been reported yet, despite its importance in gas separation since humidity is present in most industrial streams such as natural or flue gas.

The water adsorption capabilities of MOFs and their hydrothermal stability have been mainly investigated by experimental techniques, including water or N_2 adsorption, powder X-ray diffraction (XRD), scanning or transmission electron microscopies and Fourier-transform infrared (IR) spectroscopy as well as modelling approaches such as molecular dynamics and density functional theory (DFT).[9,11] These usual techniques have notably shown that in Zr-based MOFs, water molecules at low water pressure are primarily adsorbed *via* hydrogen bonding with the μ_3-OH groups of Zr clusters. As the pressure increases, additional water molecules form hydrogen bonds with the already adsorbed water molecules, fostering the development of water clusters. This process continues until the clusters reach their maximum growth capacity.[17,18] Furthermore, defects in the form of missing linkers influence the adsorption of water in UiO-66(Zr) MOF.[19–21]

Solid-state NMR spectroscopy is also a powerful technique to study water adsorption in MOFs and their hydrothermal stability since it allows the detection of defects or amorphous phases, which are not observed by diffraction techniques.[22–27] In particular, for UiO-66(Zr), ^{1}H NMR showed the formation of hydrogen bonds between water and Zr–OH groups and the exchange of hydrogen atoms between those species,[26] whereas the observation of the ^{17}O isotope demonstrated the exchange of oxygen atoms between water and the three distinct oxygen sites, μ_3-OH, μ_3-O^{2-} and COO^-, of $Zr_6O_4(OH)_4$ clusters.[27]

Nevertheless, to the best of our knowledge, solid-state NMR has never been employed in Zr-based MOFs to observe the changes in the local environment of Zr atoms induced by water adsorption or Zr-carboxylate bond hydrolysis. The observation of ^{91}Zr sites by NMR is challenging since this spin-5/2 isotope has a low natural abundance (11.22%), a low gyromagnetic ratio ($\gamma(^{91}Zr)/\gamma(^1H) = 9.3\%$) and a significant electric quadrupole moment, eQ with e the elementary charge and $Q = -17.6$ fm^2 (in comparison with -2.56 fm^2 for the ^{17}O isotope).[28] Consequently, NMR studies of these isotopes have been limited initially to sites with high local symmetry leading to small quadrupolar interaction.[29] The NMR observation of ^{91}Zr nuclei subject to large quadrupolar interaction (up to 44.7 MHz in K_2ZrF_6)[30] has been unlocked by the advent of high-field NMR magnets (up to 30 T)[30] along with pulse sequences suitable for the acquisition of wide NMR lines, such as the quadrupolar Carr–Purcell Meiboom–Gill (QCPMG) pulse sequence[31] and its variant using wideband uniform-rate smooth truncation (WURST) shaped pulses with increased excitation bandwidth[32] and piecewise acquisition of 1D NMR spectra, also termed variable-offset cumulative spectroscopy (VOCS).[31] These approaches have allowed the probing of Zr local environments in different classes of materials,[28] including zirconium oxides,[33] phosphates,[34,35] silicates,[36] halides[30] and coordination complexes.[31,37,38] Nevertheless, the number of ^{91}Zr NMR spectra reported in the literature has remained small. In particular, ^{91}Zr NMR spectra have only been reported for two MOFs so far: MIL-140A[39] and PCN-221.[40] In MIL-140A, the zirconium center resides in a low symmetrical ZrO_7 environment leading to a large C_Q value of 35 MHz, whereas in PCN-221, the authors distinguished four different ^{91}Zr signals corresponding to various coordinations of the zirconium nuclei. As far as we know, ^{91}Zr NMR has never been applied to probe water adsorption and stability of MOFs.

We compare herein the stability under steam flow at different temperatures of three Zr-based MOFs, UiO-66(Zr), UiO-66-Fum(Zr) (also called MOF-801) and UiO-67-NH_2, built from three distinct organic linkers, terephthalate, fumarate and 2-amino-[1,1′-biphenyl]-4,4′-dicarboxylate, with different sizes and affinity with water (see Table 1, Fig. S1 and S2†) using ^{91}Zr solid-state NMR spectroscopy as well as DFT calculations of NMR parameters. In particular, we investigate how the exposure to steam flow alters the local environment of ^{91}Zr nuclei.

2. Experimental methods

2.1. Synthesis

2.1.1 UiO-66. UiO-66 synthesis was up-scaled from the reported procedure[13] and adjusted for a reaction volume of 1 L so

Table 1 Characteristics of the MOF studied in this article

Name	Ligand	Structure of the ligand	Window pore size (Å)	Zr concentration (atom per nm^3)	Reference
UiO-66	Terephthalate	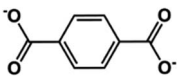	6	2.7	13
UiO-66-Fum	Fumarate	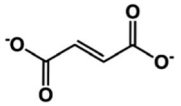	4	2.8	41
UiO-67-NH_2	2-Amino-[1,1′-biphenyl]-4,4′-dicarboxylate	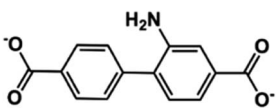	8	1.2	42

that the obtained amount of compound was sufficient for the steam flow treatments at five distinct temperatures. For this synthesis, 8 g of zirconium(IV) chloride ($ZrCl_4$, Sigma-Aldrich, 99%) and 11.2 g of terephthalic acid, also called 1,4-benzenedicarboxylic acid (H_2BDC, Sigma-Aldrich, 98%), were dissolved in 650 mL of *N*,*N*′-dimethylformamide (DMF, Sigma-Aldrich, 99.8%). The reactor was then heated at 120 °C for 24 h after a temperature ramp-up time of 1 h and allowed to cool down to room temperature in an oven. The MOF was then centrifuged and washed successively twice with DMF and twice with ethanol. Finally, the compound was activated by heating at 150 °C for 12 h, then transferred rapidly to a glovebox under an argon atmosphere.

2.1.2 UiO-66-Fum. UiO-66-Fum was synthesized according to the reported procedure.[41] Nevertheless, the quantities of reactants were increased to obtain a reaction volume of 1 L in order to produce an amount of MOF sufficient for the five steam treatments at different temperatures. In a 1 L vial, we introduced 1.2 g of $ZrCl_4$, 1.705 g of fumaric acid ($C_4H_4O_4$, Sigma-Aldrich, 98%), 5.78 mL of formic acid (HCOOH, Sigma-Aldrich, 97%), which was used as a modulator to enhance the crystallinity of the solid,[43] and 200 mL of DMF. The reaction mixture was then heated at 120 °C for 24 hours after a temperature ramp-up time of 1 h and then cooled down to room temperature in an oven. Subsequently, the MOF underwent a centrifugation and four rounds of washing (once with DMF and three times with ethanol) before being dried overnight at 60 °C. Activation was performed through three cycles of treatment with DMF and ethanol followed by heating at 130 °C overnight in a vacuum oven. Finally, the MOF was stored within a glovebox.

2.1.3 UiO-67-NH_2. In a 20 mL vial, 100 mg of $ZrCl_4$ was introduced, before the addition of 220 mg of 2-amino-[1,1′-biphenyl]-4,4′-dicarboxylic acid (H_2BPDC-NH_2), 1.5 g of benzoic acid (C_6H_5COOH, Sigma 99.5%) and 10 mL of DMF. Benzoic acid was used as a modulator. The vial was closed and subsequently subjected to a temperature of 130 °C for 48 h after a 1 h ramp-up. Following this, the temperature was decreased down to room temperature in an oven. The MOF was isolated through centrifugation, then immersed in DMF for 3 days and then 3 additional days in dichloromethane (CH_2Cl_2, Sigma-Aldrich, 99.8%). Subsequently, the MOF was centrifuged, dried in an oven at 100 °C and finally transferred into a glovebox.

2.2. Water steam stability experiments

The three MOFs, UiO-66(Zr), UiO-67-NH_2 and UiO-66-Fum, were exposed to a steam flow at different temperatures (80, 100, 150 and 200 °C) produced by a steam generator following a procedure previously reported (the setup is displayed in Fig. S2†).[25] In particular, the water and argon flows were respectively equal to 5 g h^{-1} and 15 L_n h^{-1} where L_n denotes normal liter. After this treatment, the compounds were stored in a glovebox until their characterization to limit additional exposure to water. In view of the expected stabilities of the materials, we choose to study the steam stability of the UiO-66 after seven days of exposure, whereas 24 h of exposure was used for UiO-67-NH_2 and UiO-66-Fum.

2.3. Solid-state NMR

The NMR experiments were carried out in the NMR facility of the advanced characterization platform of the Chevreul institute. The 1D ^{1}H and ^{13}C NMR spectra were recorded at 9.4 T, *i.e.* ^{1}H and ^{13}C Larmor frequencies of 400 and 100 MHz, respectively, without temperature regulation using a wide-bore Bruker spectrometer equipped with an AVANCE NEO console and a 3.2 mm triple-resonance probe used in double-resonance mode. All the samples were packed into a 3.2 mm ZrO_2 rotor in a glovebox to avoid contact with humidity and spun at 20 kHz.

The 1D ^{1}H NMR spectra were acquired using a DEPTH pulse sequence[44] to avoid a background signal. The radiofrequency (rf) nutation frequency on the ^{1}H channel was 90 kHz. The 1D ^{1}H NMR spectra resulted from averaging 16 transients with a recovery delay of 5 s. The ^{1}H isotropic chemical shifts were externally referenced to tetramethylsilane (TMS) (0 ppm) using the resonance of adamantane at 1.8 ppm as a secondary reference.

The 1D ^{13}C spectra were recorded using a ^{1}H→^{13}C cross-polarization under the magic angle spinning (CPMAS) pulse sequence with an excitation $\pi/2$ pulse of 3.4 μs. During the contact time of 2 ms, the nutation frequency on the ^{13}C channel was equal to 60 kHz, whereas the ^{1}H nutation frequency was ramped from 36 to 73 kHz. SPINAL-64 ^{1}H decoupling[45] with a nutation frequency of 90 kHz was applied during the acquisition. The 1D ^{1}H→^{13}C CPMAS spectra resulted from averaging 2048 transients with a recovery delay of 5 s. The ^{13}C isotropic chemical shifts were externally referenced to tetramethylsilane (TMS) (0 ppm) using the CH_2 resonance of adamantane at 38.5 ppm as a secondary reference.

The 1D ^{91}Zr NMR spectra were recorded at 18.8 T, *i.e.* ^{91}Zr Larmor frequency of 74.4 MHz, and 140 ± 5 K (except in Fig. 2) on a standard-bore Bruker spectrometer equipped with an AVANCE NEO console and a 4 mm double-resonance PhoenixNMR static probe. The samples for NMR analysis were packed in a 4 mm tube in a glovebox to prevent contact with moisture. The samples were cooled down using an evaporator of liquid nitrogen, which was connected to the probe. The sample temperature was stabilized using the probe heater and thermocouple, and calibrated through measurement of the ^{207}Pb isotropic chemical shift of $Pb(NO_3)_2$.[46] We assumed that the linear dependence of this parameter with temperature over the range of 143 to 423 K reported in ref. 46 is still valid at 140 K. ^{91}Zr spectra were acquired using the quadrupolar Carr-Purcell Meiboom-Gill (QCPMG) pulse sequence using WURST pulses.[32,37] The WURST pulse lengths lasted 50 μs with a frequency sweep of 1 MHz and a maximal rf field amplitude of 14 kHz. This WURST-QCPMG sequence was able to excite the full ^{91}Zr central transition (CT) of the investigated MOFs. The 1D ^{91}Zr spectra resulted from averaging 64 000 transients with a recovery delay of 1 s, leading to an experimental time of 19 h 26 min. Proton decoupling using the SW_f-TPPM[47] (swept-frequency Two-Pulse Phase Modulation) scheme with a nutation frequency of 10 kHz was applied during the acquisition. ^{91}Zr isotropic chemical shifts were indirectly referenced using

the previously published relative NMR frequencies.[48] The 1D ^{91}Zr NMR spectra were simulated using dmfit software.[49]

2.4. DFT calculations

The UiO-66-Fum and UiO-66-Fum-H_2O (with adsorbed water in the pores) configurations were obtained starting from the crystalline structures derived from the experimental XRD/Neutron data.[17] For UiO-66-Fum, μ_3-OH protons were added to obtain $Zr_6O_4(OH)_4$ clusters before relaxation of all atomic positions, keeping unit cell parameters fixed using for this purpose the Vienna *Ab Initio* Simulation Package (VASP),[50] based on the Kohn–Sham density functional theory (DFT) and using a plane-wave pseudopotential approach. A plane-wave basis set with an energy cutoff of 600 eV was employed, along with the Perdew–Burke–Ernzerhof (PBE) exchange–correlation functional.[51] The long-range weak dispersion interactions were taken into account by the DFT-D method of Grimme (DFT-D3).[52] The electron–ion interactions were described by the projector augmented wave (PAW) method[53] in the implementation of Kresse and Joubert.[54]

For UiO-66-Fum-H_2O, water molecule positions were selected respecting site occupancies inducing possible H-bonding with some of the μ_3-OH protons (ESI Fig. S11†). As done previously, all atomic positions were relaxed, keeping unit cell parameters fixed.

For UiO-67-NH_2, we started from its previously reported crystal structure (CCDC 2179854)[55] whereby we considered its primitive cell rather than the cubic structure because of its significantly smaller volume (4803.5 Å^3 *vs.* 19 214.4 Å^3). Once converted into space group P1, the model structure was prepared manually for further geometry optimization by eliminating crystallographically equivalent linkers and redundant atoms in the Zr-oxoclusters, while keeping only one –NH_2 functional group per linker (ESI Fig. S12†). Geometry optimizations were performed by keeping cell parameters fixed while relaxing all atom positions until the forces were smaller than 0.01 eV Å^{-1} and the self-consistent field (SCF) convergence criterion is below 10^{-5} eV. The Brillouin zone integration was performed at the Γ point using a *k*-spacing of 0.406 × 0.406 × 0.406 per Å.

The NMR chemical shift calculations were performed on the models built with VASP within the DFT formalism using the QUANTUM-ESPRESSO (QE) software.[56] The PBE generalized gradient approximation[51] was used and the valence electrons were described by norm conserving pseudopotentials[57] in the Kleinman–Bylander form.[58] The wave functions were expanded on a plane wave basis set with a kinetic energy cut-off of 80 Ry. The shielding tensor is computed using the Gauge Including Projector Augmented Wave (GIPAW)[59] approach, which permits the reproduction of the results of a fully converged all-electron calculation. Absolute shielding tensors are obtained. The isotropic chemical shift δ_{iso} is defined as $\delta_{iso} = \delta_{iso}^{ref} - [\sigma_{iso} - \sigma_{iso}^{ref}]$, where σ_{iso} and σ_{iso}^{ref} denote the calculated isotropic shielding of the same nucleus in the investigated and reference compounds, respectively, whereas δ_{iso}^{ref} is the experimental chemical shift of the reference, here monoclinic ZrO_2.[36] The principal components V_{xx}, V_{yy} and V_{zz} of the electric field gradient (efg) tensor are obtained by diagonalization of the tensor following the convention $|V_{zz}| \geq |V_{xx}| \geq |V_{yy}|$. The quadrupolar interaction is given as the quadrupolar coupling constant, $C_Q = eQV_{zz}/h$, and the asymmetry parameter of the efg tensor, $\eta_Q = (V_{yy} - V_{xx})/V_{zz}$, with h being the Planck constant and $Q = -17.6$ fm^2.[60]

2.5. N_2 adsorption

N_2 adsorption isotherms were recorded on a Micrometrics ASAP 2020 apparatus at 77 K. An overnight vacuum at 150 °C was done prior to the measurement. A BET model was applied in the 0.02–0.3 p/p_0 range.

2.6. XRD

The powder XRD patterns were recorded at room temperature on the XRD facility of the advanced characterization platform of the Chevreul institute using a D8 Advance A25 Bruker diffractometer with a Bragg–Brentano geometry, equipped with a LynxEye detector with Cu Kα1/α2 radiation. The 2θ range was 5–50° with a step of 0.02° and a counting time of 0.5 s per step.

2.7. IR

IR analysis was performed on a PerkinElmer Spectrum 2 instrument equipped with a single reflection diamond module (ATR). IR spectra were recorded in a 400–4000 cm^{-1} range with a 4 cm^{-1} resolution.

3. Results and discussion

3.1. Usual characterization: XRD, IR, N_2 adsorption, and ^{1}H and ^{13}C solid-state NMR

The XRD powder patterns of the three as-prepared MOFs, UiO-66, UiO-66-Fum and UiO-67-NH_2, depicted as black diffractograms in Fig. S3,† are consistent with their reported crystalline structures (ESI, Fig. S1†). After a steam flow treatment at temperatures ranging from 80 to 200 °C, the powder XRD patterns of UiO-66 and UiO-66-Fum remained unchanged. Their BET surface areas measured by N_2 adsorption also remain high after the steam flow treatment (see Fig. S5a and b in the ESI†), which confirms the preservation of their microporous structure. IR and ^{13}C NMR spectra, shown in Fig. S4a, b, S6a and b,† also confirm the stability of UiO-66 and UiO-66-Fum after the steam flow treatment. The high stability of these MOFs under steam flow is consistent with that reported in liquid water[13,16,61] or under static vapor.[14,15]

Conversely, UiO-67-NH_2 exhibits a significant reduction in crystallinity at 80, 100 and 150 °C. However, its crystalline structure is retained when exposed to a steam flow at 200 °C. These XRD data (Fig. S3c†) agree with BET surface areas reported in Fig. S5c.† These results suggest a complete collapse of the crystalline microporous structure of UiO-67-NH_2 MOF after steam flow treatment at 80 and 100 °C leading to a non-porous amorphous phase. This loss of crystallinity leads to a distribution of the local environment, as observed by the broader NMR resonances in the ^{13}C NMR spectra (see Fig. S6c†). This lower

stability of the UiO-67-NH_2 MOF stems from (i) its larger pore and the clustering of water molecules as well as (ii) the weaker Zr–O bonds, which are distorted in the case of organic linkers derived from 1,1′-biphenyl-4,4′-dicarboxylate compared to terephthalate.[61] The collapse of the UiO-67-NH_2 MOF at temperatures ranging from 80 to 150 °C but not at 200 °C is counterintuitive but has also been reported for the HKUST-1 MOF.[25]

The 1D ^{1}H NMR spectra of UiO-66 are shown in Fig. 1a and are dominated by the signal of aromatic protons of the terephthalate ligand at 8 ppm. The most intense peaks in the range 0.5–3 ppm are ascribed to Zr–OH groups. The isotropic chemical shift of these protons is known to increase by the formation of hydrogen bonds, notably with water.[26] For instance, the spectrum of as-prepared UiO-66 exhibits peaks at 0.6 and 3 ppm assigned to isolated and hydrogen-bonded Zr–OH groups.[26,62] Furthermore,

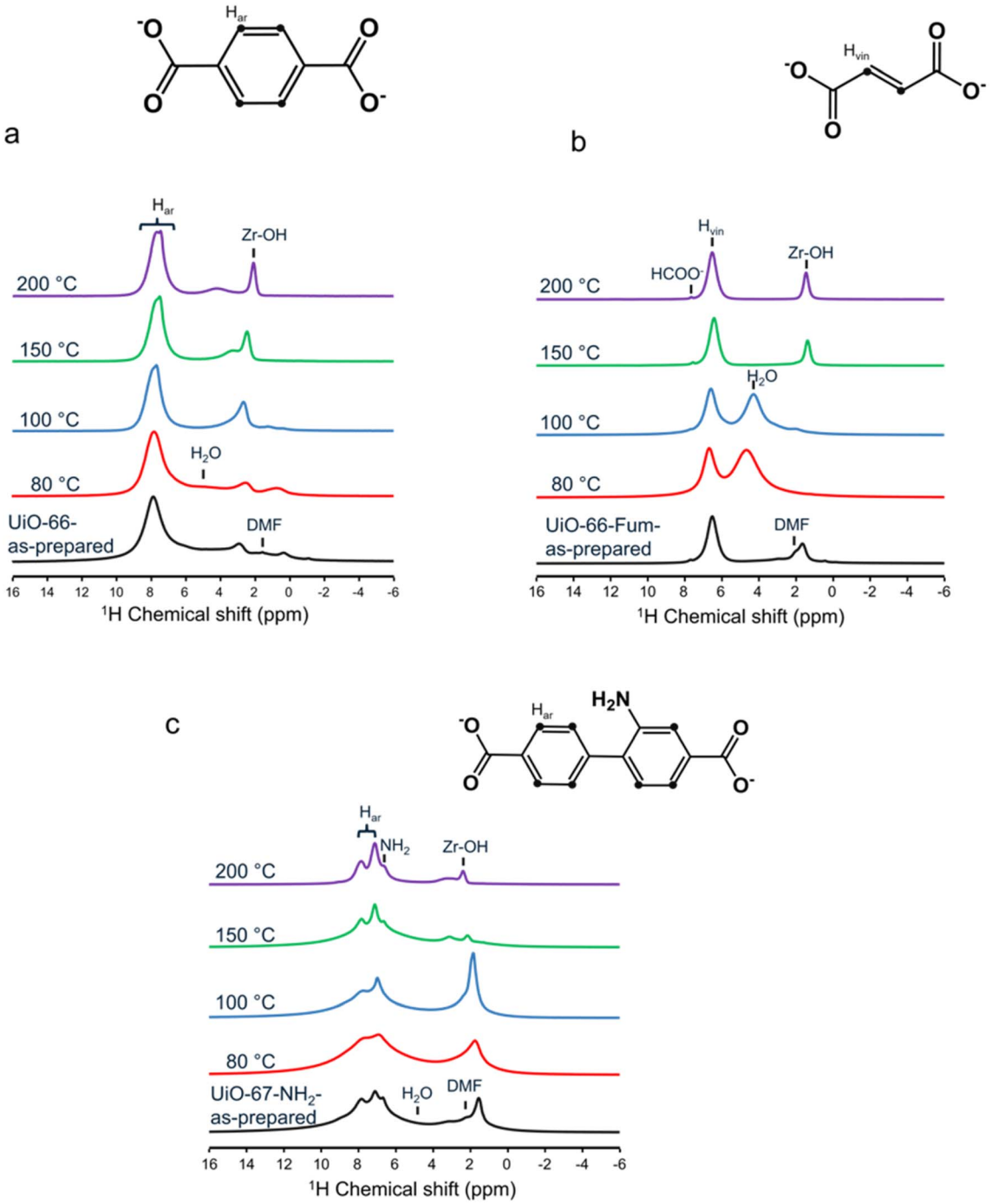

Fig. 1 1D ^{1}H NMR spectra of the (a) UiO-66, (b) UiO-66-Fum and (c) UiO-67-NH_2 MOFs: as-prepared materials (black), and after steam flow treatment at 80 (red), 100 (blue), 150 (green) and 200 °C (purple).

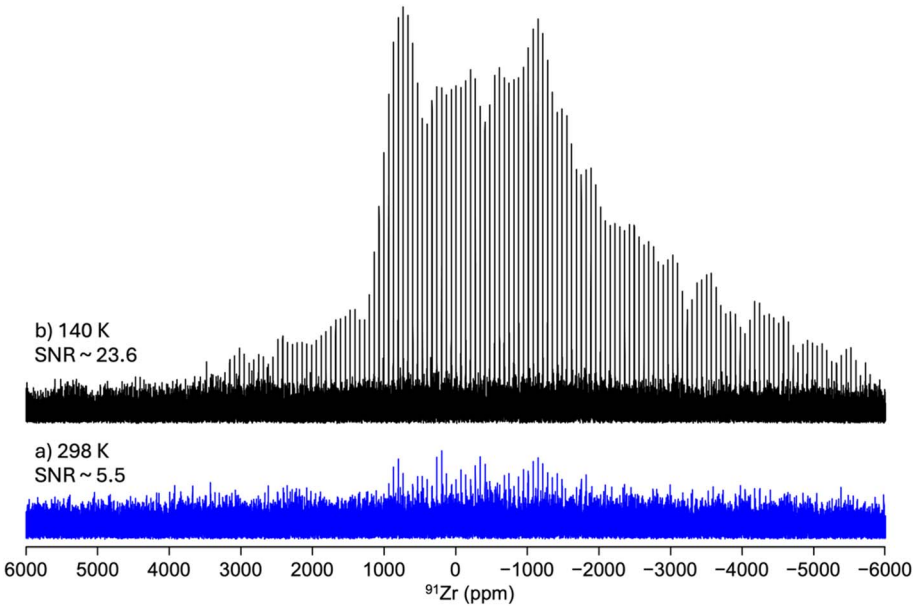

Fig. 2 1D ^{91}Zr WURST-QCPMG NMR spectra of activated UiO-66 recorded at $B_0 = 18.8$ T and (a) 298 and (b) 140 K under static conditions.

the most intense Zr–OH peak is more shielded when the temperature of steam flow increases from 100 to 200 °C, indicating that these groups form weaker hydrogen bonds, as a result of more limited water condensation in the MOF pores at high temperature. The peak at 1.6 ppm is assigned to the methyl groups of residual DMF molecules. This signal is shielded by the current in the aromatic rings of terephthalate linkers.[26,63] The signal of the DMF carbonyl group is masked by those of water and

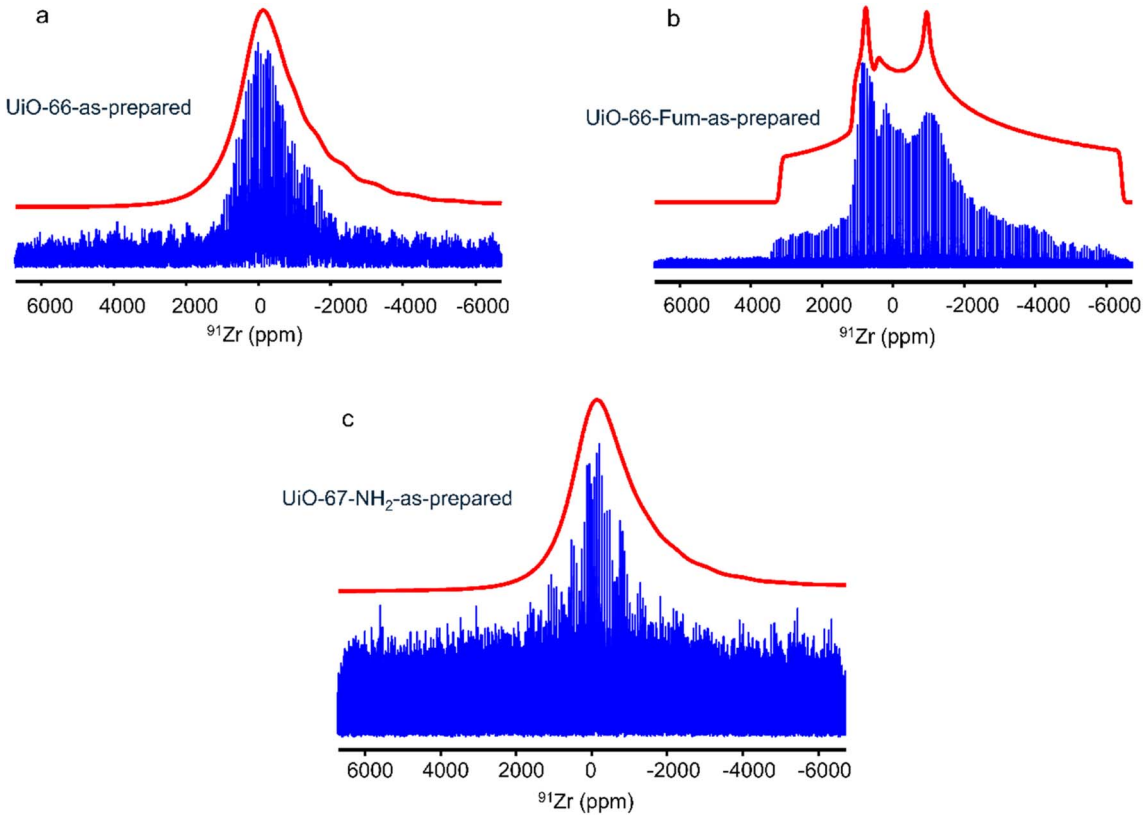

Fig. 3 Experimental 1D ^{91}Zr WURST-QCPMG NMR spectra (in blue) of the as-prepared (a) UiO-66, (b) UiO-66-Fum and (c) UiO-67-NH_2 recorded under static conditions at $B_0 = 18.8$ T and 140 K along with their simulated envelope (in red).

aromatic protons. The DMF signals disappear after thermal treatment in agreement with IR spectra. The spectrum of UiO-66 treated with steam flow at 80 °C also exhibits a broad signal near 5 ppm ascribed to adsorbed water molecules. The intensity of this signal decreases with increasing steam temperature. For the sample treated at 200 °C, the water signal is narrower and resonates at a lower chemical shift (4 ppm). The smaller linewidth suggests smaller ^{1}H–^{1}H dipolar interactions, whereas shielding indicates longer OH···O distances.[64,65] These two observations are consistent with less water condensation in UiO-66 pores at 200 °C.

Fig. 1b displays the 1D ^{1}H MAS NMR spectra of UiO-66-Fum. The intense peak at 6.5 ppm is ascribed to the vinylic protons of the fumarate linkers, whereas the Zr–OH groups produce resonances between 1.5 and 3 ppm. For the as-prepared sample and that treated with steam at 100 °C, the signal of the methyl groups of DMF is also visible in agreement with IR spectra (ESI, Fig. S4b†). The spectra of the samples treated with steam at 80 and 100 °C exhibit an intense signal near 5 ppm of water protons. The higher intensity of this peak compared to that of the UiO-66 compound treated at the identical temperature is consistent with the higher hydrophilicity of UiO-66-Fum with respect to UiO-66,[2] most probably because of the size of the window pore diameter. For the UiO-66-Fum treated at 80 and 100 °C, the Zr–OH peak disappears because of the exchange with water. Conversely, at 150 and 200 °C, the water peak vanishes, and the Zr–OH peak is shielded down to 1.5 ppm since it forms weaker hydrogen bonds.

The ^{1}H NMR spectrum of UiO-67-NH_2 displayed in Fig. 1c exhibits signals between 7 and 8 ppm assigned to the aromatic protons of the linker and a peak at 6.8 ppm ascribed to the NH_2 group, whereas Zr–OH protons resonate at chemical shifts ranging between 1.6 and 3.2 ppm. The steam flow treatment at 80 and 100 °C broadens the ^{1}H resonances since the collapse of the MOF crystalline structure results in a distribution of local environments.[22,25] This observation is consistent with ^{13}C NMR spectra (shown in Fig. S6c†). After steam treatment at 150 and 200 °C, the ^{1}H resonances remain narrow but the Zr–OH peaks are deshielded owing to the formation of hydrogen bonds with water.

3.2. ^{91}Zr solid-state NMR

3.2.1 As-prepared MOFs. The ^{91}Zr NMR spectrum of activated UiO-66 was initially acquired at 298 K using the WURST-QCPMG pulse sequence. Nevertheless, the fast dynamics of

Table 2 Calculated ^{91}Zr NMR parameters of UiO-66, UiO-66-Fum, UiO-66-Fum-H_2O and UiO-67-NH_2 MOFs along with the experimental ^{91}Zr NMR parameters of these MOFs, as-prepared and after steam treatment at different temperatures. Note that for the calculated ^{91}Zr NMR parameters, the protons of the $Zr_6O_4(OH)_4$ cluster present in all these MOFs have an occupancy of 0.5, leading to a relaxation of the atomic positions in space group P1. This partial occupancy induces variations in the calculated ^{91}Zr NMR parameters between the slightly inequivalent zirconium positions in UiO-67-NH_2, UiO-66-Fum and UiO-66-Fum-hydrated structures. Averaged values are indicated in this table but complete values can be found in Tables S4 to S6. The errors on the calculated chemical shifts and C_Q constants were estimated through the comparison between calculated and experimental parameters for a series of reference compounds (see Table S7 and Fig. S14 in the ESI). The experimental ^{91}Zr NMR parameters were obtained by simulating the 1D ^{91}Zr NMR spectra using a single quadrupolar lineshape, except for samples denoted by an * symbol for which a Czjzek model was employed. For those samples, the reported C_Q constants are the peak values of the C_Q constant. As the mean η_Q parameter is always equal to 0.61 for this model, it is not given[68]

Sample	Temp. of steam treatment (°C)	δ_{iso} (ppm)	C_Q (MHz)	η_Q	δ_{11} (ppm)	δ_{22} (ppm)	δ_{33} (ppm)
UiO-66							
Calculated	—	−55 (±20)	25.8 (±3)	0.7	−158 (±20)	−126 (±20)	119 (±20)
Experimental	As-prepared*	−28 (±50)	22.1	—	—	—	—
	80	−93 (±80)	29.5	0.70	—	—	—
	100	−100 (±50)	31.4	0.75	—	—	—
	150	−118 (±50)	31.8	0.75	—	—	—
	200	−120 (±50)	32.0	0.74	—	—	—
UiO-66-Fum							
Calculated	Empty pores	−47 (±20)	27.4 (±3)	0.7	−154 (±20)	−113 (±20)	127 (±20)
Calculated	H_2O in pores	−48 (±20)	26.7 (±3)	0.8	159 (±20)	−111 (±20)	126 (±20)
Experimental	As-prepared	−30	31.8	0.75	—	—	—
	80*	100 (±80)	20.4	—	—	—	—
	100*	170 (±50)	24.0	—	—	—	—
	150	−20 (±50)	32.0	0.75	—	—	—
	200	−20 (±50)	32.5	0.75	—	—	—
UiO-67-NH_2							
Calculated		−55 (±20)	27.3 (±3)	0.7	−167 (±20)	−127 (±20)	128 (±20)
Experimental	As prepared*	−20 (±100)	21.3	—	—	—	—
	80	—	—	—	—	—	—
	100	—	—	—	—	—	—
	150*	−25 (±100)	25	—	—	—	—
	200*	−25 (±100)	25	—	—	—	—

phenylene ring librations,[66] adsorbed water and DMF molecules result in fast decay of the signal envelope in a spin-echo experiment, preventing the acquisition of multiple echoes in the QCPMG scheme and resulting in poor signal-to-noise ratio (SNR) (see Fig. 2 and ESI Table S2†). Previous ^{2}H NMR experiments on UiO-66 have indicated that the rotation of benzene rings is strongly slowed down below 213 K.[67] Therefore, the sample temperature was lowered down to 140 K, *i.e.* −133 °C, to reduce the mobility and hence to lengthen the decay of the signal envelope. This decreased temperature enhances the signal-to-noise ratio by a factor of up to 5-fold. Hence, all 1D ^{91}Zr NMR spectra of the investigated Zr-based MOFs were then acquired at 140 K.

Fig. 3 shows the 1D ^{91}Zr NMR spectra of the as-prepared UiO-66, UiO-66-Fum and UiO-67-NH_2 MOFs. Their SNR decreases with increasing length of the organic linkers, which results in decreasing concentration of Zr atoms per unit cell (see Table 1). These QCPMG spectra exhibit spikelets because of the acquisition of an echo train. The envelope of these spectra obtained by the Fourier transform (FT) of the sum of the echoes is shown in ESI Fig. S7–S9.† The spectrum of UiO-66-Fum exhibits a broad CT with several discontinuities, which can be simulated with a quadrupolar lineshape with an isotropic chemical shift $\delta_{iso} = -30$ ppm, $C_Q = 31.8$ MHz and $\eta_Q = 0.75$ (see Table 2). Conversely, the spectra of UiO-66 and UiO-67-NH_2 show narrower CT without clear discontinuities and could not be properly simulated using the quadrupolar lineshape of a single site (see Fig. S10 in the ESI†). In particular, the resonance of UiO-66 tails toward negative chemical shifts, which betrays a distribution of local environments around ^{91}Zr nuclei due to the presence of disordered adsorbed molecules of water and DMF in the MOF micropores. These adsorbed molecules affect the efg at the position of ^{91}Zr nuclei. Owing to this distribution of quadrupolar interaction, these spectra were simulated using a Czjzek model.[68]

These differences between the three MOFs are unexpected since they are built from the same $Zr_6O_4(OH)_4$ clusters and their single Zr crystallographic site exhibits similar distances between the metal center and the eight connected oxygen atoms (ESI Table S1†).[17,69,70] The narrower lineshapes for UiO-66 and UiO-67-NH_2 could stem from the presence of more DMF and other adsorbed molecules such as water in their pores compared to UiO-66-Fum, as suggested for the former MOFs by larger relative intensities between 2 and 6 ppm in the ^{1}H spectra (see Fig. 1) and the more intense DMF band at 1655 cm^{-1} (see Fig. S4†). These adsorbed molecules, which lack long-range order, induce a distribution of the local environment and reduce the electric field gradient at the position of the ^{91}Zr nuclei, thus decreasing the quadrupolar interaction. The lower signal-to-noise ratio for UiO-67-NH_2 stems from both (i) the

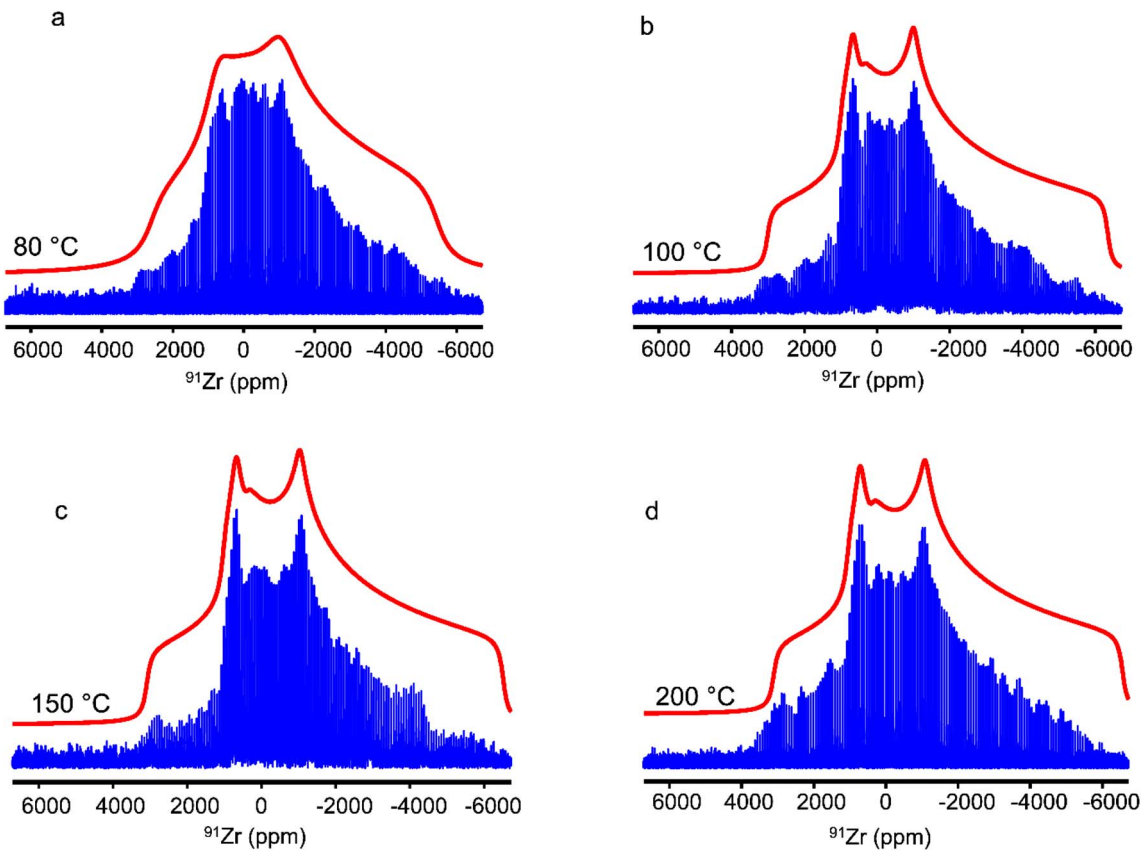

Fig. 4 Experimental 1D ^{91}Zr WURST-QCPMG NMR spectra (in blue) of UiO-66 submitted to steam flow during 7 days at (a) 80, (b) 100, (c) 150 and (d) 200 °C recorded under static conditions at $B_0 = 18.8$ T and 140 K along with their simulated envelope (in red).

lower concentration of Zr atoms in that compound built from a longer linker, as well as (ii) the faster decay of the QCPMG echo envelope owing to higher mobility, including the rotation of the amino group.

The ^{91}Zr NMR parameters of these MOFs have also been calculated using the DFT-GIPAW method (see Table 2). It can be noted that the nature of the linker seems to have a small impact on the calculated ^{91}Zr NMR parameters of the $Zr_6O_4(OH)_4$ cluster. Nevertheless, a comparison with experimental parameters is difficult since the DFT calculations were performed at 0 K, whereas the NMR spectra were acquired at 140 K and temperature affects the atomic-level dynamics and hence the NMR interactions. In addition, most crystal structures used for the calculations do not contain solvent molecules in the pores, in contrast to the investigated sample.

3.2.2 After steam treatment. The 1D ^{91}Zr QCPMG NMR spectra of UiO-66 after steam treatment at 80, 100, 150 and 200 °C are shown in Fig. 4. Their experimental envelope is also displayed in ESI Fig. S7.† These spectra are significantly broader than those of the as-prepared UiO-66 and exhibit more pronounced discontinuities, even if the horns of the CT are less marked for the sample treated at 80 °C. These spectra can be simulated by a quadrupolar lineshape with -93 ppm $\leq \delta_{iso} \leq -120$ ppm, 29.5 MHz $\leq C_Q \leq$ 32.0 MHz and 0.70 $\leq \eta_Q \leq$ 0.75. As seen in Table 2, these NMR parameters agree reasonably well with those calculated from the crystal structure of this MOF solved from single-crystal X-ray diffraction.[69] This result indicates that the local environment of Zr atoms in these treated UiO-66 MOFs is mostly the same as in the crystal structure. Hence, steam treatment removes most of the adsorbed molecules and the inorganic cluster of UiO-66 remains stable after steam treatment during 7 days at temperatures ranging from 80 to 200 °C. The larger relative intensity near 0 ppm for the sample treated with steam at 80 °C indicates that some ^{91}Zr nuclei still have NMR parameters similar to those of the as-prepared UiO-66 and a small amount of adsorbed molecules remains in the pores. Hence, this spectrum could in principle be simulated as the sum of a quadrupolar lineshape, ascribed to the ^{91}Zr nuclei without adsorbed molecules in their vicinity, and a lineshape calculated using a Czjzek model[68] produced by Zr sites close to residual adsorbed molecules. Nevertheless, this simulation [not shown] employs a large number of parameters, which result in large error bars.

Fig. 5 shows the 1D ^{91}Zr QCPMG spectra of UiO-66-Fum after steam treatment, and their envelopes are displayed in Fig. S8.† The ^{91}Zr signal of this MOF is not significantly altered by steam treatment at 150 and 200 °C. This result indicates that steam treatment at these temperatures does not cause either water adsorption or alteration of the crystal structure. Conversely,

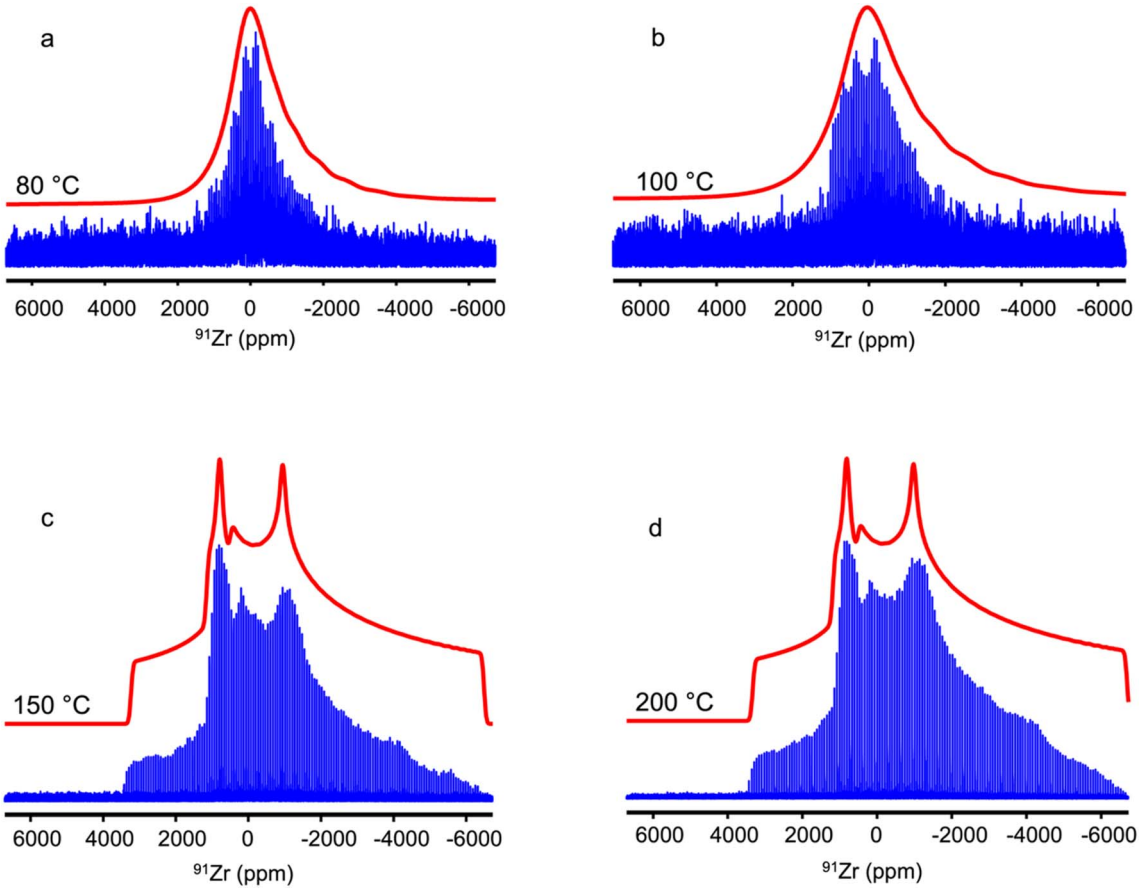

Fig. 5 Experimental 1D ^{91}Zr WURST-QCPMG NMR spectra (in blue) of UiO-66-Fum submitted to steam flow during 24 h at (a) 80, (b) 100, (c) 150 and (d) 200 °C recorded under static conditions at $B_0 = 18.8$ T and 140 K along with their simulated envelope (in red).

steam treatment at 80 °C results in a narrowing of the CT stemming from reduced quadrupolar coupling constant and the absence of pronounced discontinuities, which suggests a distribution of local environments. Therefore, the ^{91}Zr NMR spectrum of UiO-66-Fum after steam treatment at 80 °C can be convincingly simulated using a Czjzek model (compare Fig. 5b and S10b†). As this sample is crystalline (see Fig. S3b†), the distribution of efg tensor stems, like for as-prepared UiO-66, from the disorder of molecules adsorbed in the pores. This observation is consistent with the 1D ^{1}H spectrum, which shows the adsorption of water molecules in the pores after steam treatment at 80 °C (see Fig. 1). The ^{91}Zr NMR spectrum of the UiO-66-Fum after a steam treatment at 100 °C is broader than that treated at 80 °C and exhibits small discontinuities. Nevertheless, it remains narrower than the spectrum of the as-prepared sample. The spectrum of the sample treated at 100 °C cannot be perfectly simulated using either a single quadrupolar lineshape (see Fig. S10b†) or a Czjzek model (see Fig. 5b). Like the spectrum of UiO-66 treated at 80 °C, it should be simulated as the sum of a Czjzek lineshape produced by ^{91}Zr nuclei close to disordered adsorbed molecules and a quadrupolar lineshape due to ^{91}Zr nuclei without adsorbed molecules in their vicinity. Nevertheless, this simulation employing two distinct lineshapes [not shown] results in best–fit parameters with large error bars owing to the lack of resolution of the ^{91}Zr NMR spectrum. We can also notice the smaller number of QCPMG echoes detected for the samples treated at 80 and 100 °C. This reduced number of echoes may stem from an increased density of protons around the ^{91}Zr nuclei owing to the adsorption of water in the pores, as observed in the ^{1}H NMR spectra of Fig. 1b. Calculations were performed using the published structure of UiO-66-Fum.[17] The authors have also resolved a structure of this compound containing adsorbed water. The calculated values of the quadrupolar parameters of both structures are shown in Table 2 and ESI Fig. S11, S12, Tables S4 and S5.† They show that the adsorption of water within the UiO-66-Fum broadens the distribution of $\delta_{iso}(^{91}Zr)$ and C_Q values. Nevertheless, the reduction in the average C_Q value for UiO-66-Fum-H_2O with respect to UiO-66-Fum is much smaller than that between the as-prepared UiO-66-Fum and the same sample after steam flow treatment at 80 and 100 °C, probably because those samples contain a larger amount of water than the UiO-66-Fum-H_2O model.

The ^{91}Zr NMR spectra of UiO-67-NH_2 subjected to steam treatment at various temperatures are displayed in Fig. 6, whereas their envelopes are shown in ESI Fig. S9.† The spectra of the samples treated at 150 and 200 °C exhibit a broad signal around 0 ppm like that of the as-prepared sample shown in

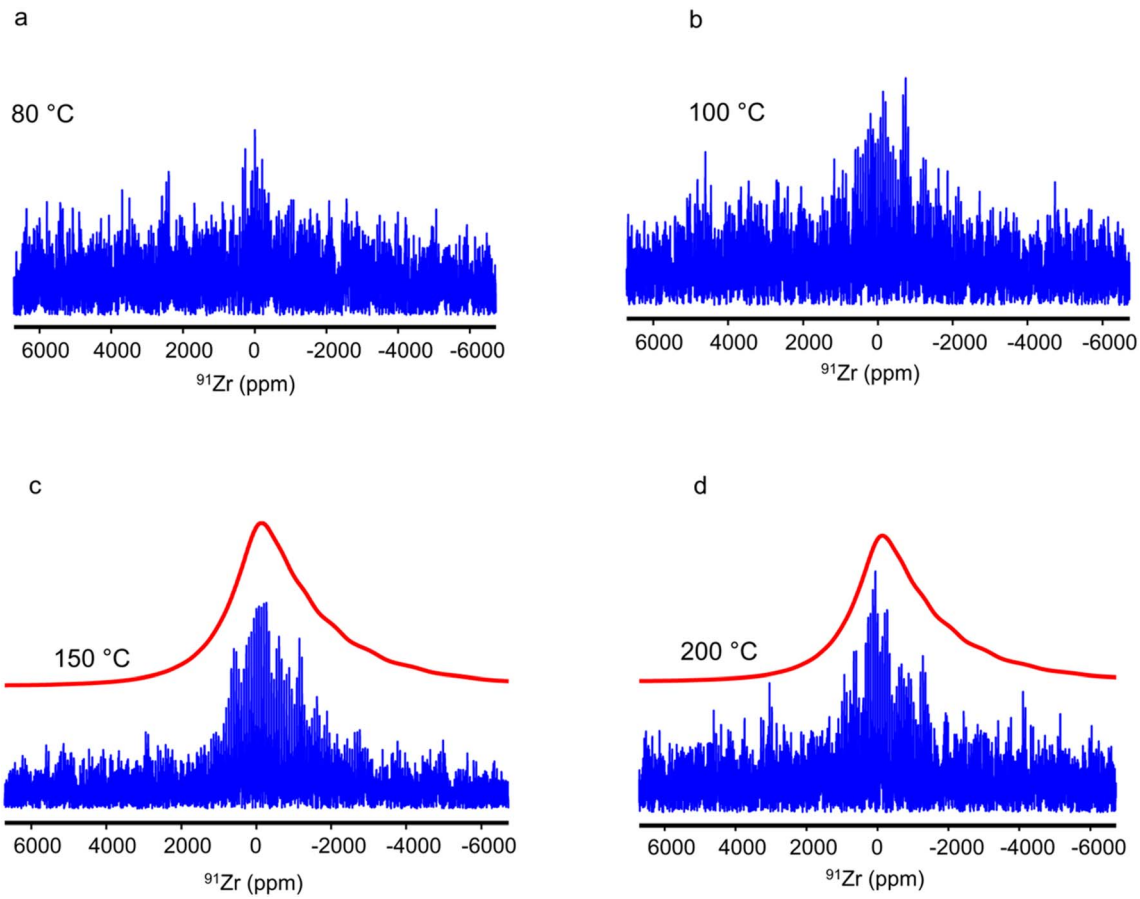

Fig. 6 Experimental 1D ^{91}Zr WURST-QCPMG NMR spectra (in blue) of UiO-67-NH_2 submitted to steam flow during 24 h at (a) 80, (b) 100, (c) 150 and (d) 200 °C recorded under static conditions at $B_0 = 18.8$ T and 140 K along with their simulated envelope (in red).

Fig. 3c. Owing to their low SNR, they are challenging to simulate. We can only notice that their lineshape is compatible with that calculated using a Czjzek model and parameters similar to those employed for the simulation of ^{91}Zr NMR spectra of the as-prepared UiO-66 and UiO-67-NH_2. Stronger deviations are observed between these experimental spectra and those simulated using a single quadrupolar lineshape with the NMR parameter similar to those calculated using DFT (see Fig. S10e and f and Table S3† in the ESI). Hence, we can assume that UiO-67-NH_2 treated at 150 and 200 °C contain, like as-prepared UiO-66 and UiO-67-NH_2, a distribution of the ^{91}Zr local environment owing to disordered adsorbed water molecules in their pores. In contrast, the ^{91}Zr NMR signal is hardly detected for samples treated at temperatures ranging from 80 to 100 °C, whereas based on DFT calculations, the ^{91}Zr nuclei are subject to similar quadrupolar interactions for UiO-66, UiO-66-Fum and UiO-67-NH_2 (see Table 2). Hence, the vanishing or weak ^{91}Zr signal after steam treatment at 80 or 100 °C must result from the collapse of the MOF crystalline structure, which is inferred from XRD and surface area measurements (see ESI Fig. S3 and S5†). The formation of amorphous materials broadens the NMR signal and hence decreases its intensity. Furthermore, a reduced number of echoes in the QCPMG experiment were detected for these samples (see Table S2†), which suggests increased dynamics around ^{91}Zr nuclei. In particular, the collapse of the MOF crystalline structure and the partial hydrolysis of Zr–O bonds may accelerate the motions of organic linkers, which exhibit hindered rotation at low temperature in the MOF.[67] The vanishing or weak ^{91}Zr NMR signal for the samples treated at 80 and 100 °C is consistent with the resonance broadening observed for the ^{1}H and ^{13}C NMR spectra (see Fig. 1 and S6†). These results suggest that the amorphous phase contains both Zr atoms and organic linkers.

As mentioned above, the lower stability of the UiO-67-NH_2 MOF compared to UiO-66 and UiO-66-Fum stems from weaker Zr–O bonds and larger pores, which facilitates the formation of water clusters around the Zr-carboxylate bonds and hence their hydrolysis.[61] Furthermore, the collapse of the crystalline structure of the UiO-67-NH_2 MOF in the presence of steam flow up to 100 °C but not at 200 °C is counterintuitive but falls in line with previous observations for a Cu-based HKUST MOF.[25] At lower temperature, H_2O, or DMF condenses in the pores, which favors the formation of water clusters around the Zr–carboxylate coordination bonds and hence their hydrolysis. TGA/DSC experiments could shed light on this in the future (beyond the scope of this article). Conversely, at high temperature, the condensation of water in the MOF micropores is more limited, which prevents the formation of water clusters and consequently, the hydrolysis of coordination bonds.[61]

4. Conclusion

We investigated the adsorption of water at various temperatures of three MOFs, UiO-66(Zr), UiO-66-Fum(Zr) and UiO-67-NH_2. They are constructed from identical $Zr_6O_4(OH)_4$ clusters combined with three distinct organic linkers. The behaviour of these zirconium clusters under steam flow was examined using ^{91}Zr solid-state NMR and DFT calculations. To address the broad lineshape, we recorded WURST-QCPMG spectra at high magnetic field and low temperature (140 K). Our study demonstrates for the first time that the ^{91}Zr NMR parameters are sensitive not only to the collapse of the MOF crystalline structure but also to the adsorption of molecules, and notably water, within their pores.

Our findings reveal that UiO-66(Zr) and UiO-66-Fum(Zr) are stable at steam flow temperatures ranging from 80 to 200 °C for up to 24 h (and even 7 days for UiO-66(Zr)). In contrast, the crystalline microporous structure of UiO-67-NH_2 collapses within 24 h under steam flow at 80 to 150 °C, whereas it is preserved at 200 °C. This reduced stability of UiO-67-NH_2 is attributed to its larger pore and weaker Zr–O bonds. The structural integrity at 200 °C is likely due to limited water condensation in the pores at this higher temperature, which prevents the formation of water clusters and hence the hydrolysis of Zr–carboxylate coordination bonds.

Data availability

The data supporting the article have been included as part of the ESI.†

Author contributions

AN: performed the solid-state NMR of the fumarate and UiO-66, performed the steam treatment and the figure of the manuscript. FV: performed the solid state NMR of the UiO-67-NH_2, performed the steam treatment. RG: synthesized the samples. ML: synthesized the ligand for the UiO-67-NH_2. CV: supervised the syntheses, the N_2 adsoprtion and the XRD. TL: supervised the syntheses of the ligand and the IR. CG: performed the calculations. CMD: symmetrized the structure for the calculations. BD: supervised the low temperature experiments. JT: supervised the high-field NMR. OL: supervised the NMR and help for the writing of the manuscript. FP: managed the team, conducted the research, write the manuscript.

Conflicts of interest

There are no conflicts to declare.

Acknowledgements

The Chevreul Institute is thanked for supporting CPER projects funded by the "Ministère de l'Enseignement Supérieur et de la Recherche", the region "Hauts-de-France", the ERDF program of the European Union and the "Métropole Européenne de Lille". Financial support from the IR INFRANALYTICS FR2054 for conducting the research is gratefully acknowledged. Authors are also grateful for funding supported by contract I-site EXPAND MOFFiN and the Institut Universitaire de France. DFT NMR calculations were performed using HPC resources from GENCI-IDRIS (Grant AD010-09535).

References

1 United Nations Development Program, The Next Frontier: Human Development and the Anthropocene; USA, 2020, https://www.undp.org/belarus/publications/next-frontier-human-development-and-anthropocene.

2 H. Kim, S. Yang, S. R. Rao, S. Narayanan, E. A. Kapustin, H. Furukawa, A. S. Umans, O. M. Yaghi and E. N. Wang, Water harvesting from air with metal-organic frameworks powered by natural sunlight, *Science*, 2017, **356**(6336), 430–432, DOI: 10.1126/science.aam8743.

3 N. Hanikel, M. S. Prévot and O. M. Yaghi, MOF water harvesters, *Nat. Nanotechnol.*, 2020, **15**(5), 348–355, DOI: 10.1038/s41565-020-0673-x.

4 M. Mon, R. Bruno, J. Ferrando-Soria, D. Armentano and E. Pardo, Metal-organic framework technologies for water remediation: towards a sustainable ecosystem, *J. Mater. Chem. A*, 2018, **6**(12), 4912–4947, DOI: 10.1039/c8ta00264a.

5 D. Buzek, J. Demel and K. Lang, Zirconium Metal-Organic Framework UiO-66: Stability in an Aqueous Environment and Its Relevance for Organophosphate Degradation, *Inorg. Chem.*, 2018, **57**(22), 14290–14297, DOI: 10.1021/acs.inorgchem.8b02360.

6 F. Ahmadijokani, H. Molavi, M. Rezakazemi, S. Tajahmadi, A. Bahi, F. Ko, T. M. Aminabhavi, J. R. Li and M. Arjmand, UiO-66 metal–organic frameworks in water treatment: A critical review, *Prog. Mater. Sci.*, 2022, **125**, 100904, DOI: 10.1016/j.pmatsci.2021.100904.

7 R. M. Rego, M. D. Kurkuri and M. Kigga, A comprehensive review on water remediation using UiO-66 MOFs and their derivatives, *Chemosphere*, 2022, **302**, 138283, DOI: 10.1016/j.chemosphere.2022.134845.

8 E. Soubeyrand-Lenoir, C. Vagner, J. W. Yoon, P. Bazin, F. Ragon, Y. K. Hwang, C. Serre, J. S. Chang and P. L. Llewellyn, How Water Fosters a Remarkable 5-Fold Increase in Low-Pressure CO_2 Uptake within Mesoporous MIL-100(Fe), *J. Am. Chem. Soc.*, 2012, **134**(24), 10174–10181, DOI: 10.1021/ja302787x.

9 X. L. Liu, X. R. Wang and F. Kapteijn, Water and Metal-Organic Frameworks: From Interaction toward Utilization, *Chem. Rev.*, 2020, **120**(16), 8303–8377, DOI: 10.1021/acs.chemrev.9b00746.

10 R. P. Loughran, T. Hurley, A. Gladysiak, A. Chidambaram, K. Khivantsev, E. D. Walter, T. R. Graham, P. Reardon, J. Szanyi, D. B. Fast, *et al.*, CO_2 capture from wet flue gas using a water-stable and cost-effective metal-organic framework, *Cell Rep. Phys. Sci.*, 2023, **4**(7), 101470, DOI: 10.1016/j.xcrp.2023.101470.

11 N. C. Burtch, H. Jasuja and K. S. Walton, Water Stability and Adsorption in Metal-Organic Frameworks, *Chem. Rev.*, 2014, **114**(20), 10575–10612, DOI: 10.1021/cr5002589.

12 J. Canivet, A. Fateeva, Y. M. Guo, B. Coasne and D. Farrusseng, Water adsorption in MOFs: fundamentals and applications, *Chem. Soc. Rev.*, 2014, **43**(16), 5594–5617, DOI: 10.1039/c4cs00078a.

13 J. H. Cavka, S. Jakobsen, U. Olsbye, N. Guillou, C. Lamberti, S. Bordiga and K. P. Lillerud, A new zirconium inorganic building brick forming metal organic frameworks with exceptional stability, *J. Am. Chem. Soc.*, 2008, **130**(42), 13850–13851, DOI: 10.1021/ja8057953.

14 J. B. DeCoste, G. W. Peterson, B. J. Schindler, K. L. Killops, M. A. Browe and J. J. Mahle, The effect of water adsorption on the structure of the carboxylate containing metal-organic frameworks Cu-BTC, Mg-MOF-74, and UiO-66, *J. Mater. Chem. A*, 2013, **1**(38), 11922–11932, DOI: 10.1039/c3ta12497e.

15 K. Leus, T. Bogaerts, J. De Decker, H. Depauw, K. Hendrickx, H. Vrielinck, V. Van Speybroeck and P. Van Der Voort, Systematic study of the chemical and hydrothermal stability of selected "stable" Metal Organic Frameworks, *Microporous Mesoporous Mater.*, 2016, **226**, 110–116, DOI: 10.1016/j.micromeso.2015.11.055.

16 H. Motegi, K. Yano, N. Setoyama, Y. Matsuoka, T. Ohmura and A. Usuki, A facile synthesis of UiO-66 systems and their hydrothermal stability, *J. Porous Mater.*, 2017, **24**(5), 1327–1333, DOI: 10.1007/s10934-017-0374-5.

17 H. Furukawa, F. Gándara, Y. B. Zhang, J. C. Jiang, W. L. Queen, M. R. Hudson and O. M. Yaghi, Water Adsorption in Porous Metal-Organic Frameworks and Related Materials, *J. Am. Chem. Soc.*, 2014, **136**(11), 4369–4381, DOI: 10.1021/ja500330a.

18 M. C. Lawrence and M. J. Katz, Analysis of the Water Adsorption Isotherms in UiO-Based Metal-Organic Frameworks, *J. Phys. Chem. C*, 2022, **126**(2), 1107–1114, DOI: 10.1021/acs.jpcc.1c05190.

19 P. Ghosh, Y. J. Colon and R. Q. Snurr, Water adsorption in UiO-66: the importance of defects, *Chem. Commun.*, 2014, **50**(77), 11329–11331, DOI: 10.1039/c4cc04945d.

20 W. B. Liang, C. J. Coghlan, F. Ragon, M. Rubio-Martinez, D. M. D'Alessandro and R. Babarao, Defect engineering of UiO-66 for CO_2 and H_2O uptake - a combined experimental and simulation study, *Dalton Trans.*, 2016, **45**(11), 4496–4500, DOI: 10.1039/c6dt00189k.

21 G. Jajko, J. J. Gutiérrez-Sevillano, A. Slawek, M. Szufla, P. Kozyra, D. Matoga, W. Makowski and S. Calero, Water adsorption in ideal and defective UiO-66 structures, *Microporous Mesoporous Mater.*, 2022, **330**, 111555, DOI: 10.1016/j.micromeso.2021.111555.

22 F. Gul-E-Noor, B. Jee, A. Poppl, M. Hartmann, D. Himsl and M. Bertmer, Effects of varying water adsorption on a $Cu_3(BTC)_2$ metal-organic framework (MOF) as studied by ^1H and ^{13}C solid-state NMR spectroscopy, *Phys. Chem. Chem. Phys.*, 2011, **13**(17), 7783–7788, DOI: 10.1039/c0cp02848g.

23 F. Gul-E-Noor, D. Michel, H. Krautscheid, J. Haase and M. Bertmer, Time dependent water uptake in $Cu_3(btc)_2$ MOF: Identification of different water adsorption states by ^1H MAS NMR, *Microporous Mesoporous Mater.*, 2013, **180**, 8–13, DOI: 10.1016/j.micromeso.2013.06.033.

24 R. W. Faig, T. M. O. Popp, A. M. Fracaroli, E. A. Kapustin, M. J. Kalmutzki, R. M. Altamimi, F. Fathieh, J. A. Reimer and O. M. Yaghi, The Chemistry of CO_2 Capture in an

Amine-Functionalized Metal-Organic Framework under Dry and Humid Conditions, *J. Am. Chem. Soc.*, 2017, **139**(35), 12125–12128, DOI: 10.1021/jacs.7b06382.

25 R. Giovine, F. Pourpoint, S. Duval, O. Lafon, J. P. Amoureux, T. Loiseau and C. Volkringer, The Surprising Stability of $Cu_3(btc)_2$ Metal-Organic Framework under Steam Flow at High Temperature, *Cryst. Growth Des.*, 2018, **18**(11), 6681–6693, DOI: 10.1021/acs.cgd.8b00931.

26 F. Venel, C. Volkringer, O. Lafon and F. Pourpoint, Probing adsorption of water and DMF in UiO-66(Zr) using solid-state NMR, *Solid State Nucl. Magn. Reson.*, 2022, **120**, 101797, DOI: 10.1016/j.ssnmr.2022.101797.

27 F. Venel, R. Giovine, D. Laurencin, J. Spacková, S. Mittelette, T. X. Métro, C. Volkringer, O. Lafon and F. Pourpoint, Probing oxygen exchange between UiO-66(Zr) MOF and water using ^{17}O solid-state NMR, *Chem.–Eur. J.*, 2024, **30**, e202302731, DOI: 10.1002/chem.202302731.

28 B. E. G. Lucier and Y. Huang, Review of ^{91}Zr Solid-State Nuclear Magnetic Resonance Spectroscopy, *Annu. Rep. NMR Spectrosc.*, 2015, **84**, 233–289, DOI: 10.1016/bs.arnmr.2014.10.005.

29 T. Yamadaya and M. Asanuma, Nuclear Magnetic Resonance of ^{91}Zr in $ZrZn_2$, *Phys. Rev. Lett.*, 1965, **15**(17), 695–696, DOI: 10.1103/PhysRevLett.15.695.

30 O. Pauvert, F. Fayon, A. Rakhmatullin, S. Kramer, M. Horvatic, D. Avignant, C. Berthier, M. Deschamps, D. Massiot and C. Bessada, ^{91}Zr Nuclear Magnetic Resonance Spectroscopy of Solid Zirconium Halides at High Magnetic Field, *Inorg. Chem.*, 2009, **48**(18), 8709–8717, DOI: 10.1021/ic9007119.

31 I. Hung and R. W. Schurko, Solid-state ^{91}Zr NMR of bis(cyclopentadienyl)dichlorozirconium(IV), *J. Phys. Chem. B*, 2004, **108**(26), 9060–9069, DOI: 10.1021/jp040270u.

32 L. A. O'Dell and R. W. Schurko, QCPMG using Adiabatic Pulses for Faster Acquisition of Ultra-Wideline NMR Spectra, *Chem. Phys. Lett.*, 2008, **464**(1–3), 97–102, DOI: 10.1016/j.cplett.2008.08.095.

33 T. J. Bastow, M. E. Smith and S. N. Stuart, Observation of ^{91}Zr NMR in Zirconium-based Metals and Oxides, *Chem. Phys. Lett.*, 1992, **191**(1–2), 125–129, DOI: 10.1016/0009-2614(92)85380-s.

34 Z. M. Yan, C. W. Kirby and Y. N. Huang, Directly probing the metal center environment in layered zirconium phosphates by solid-state ^{91}Zr NMR, *J. Phys. Chem. C*, 2008, **112**(23), 8575–8586, DOI: 10.1021/jp711137c.

35 A. Sutrisno, L. Liu, J. X. Dong and Y. N. Huang, Solid-State ^{91}Zr NMR Characterization of Layered and Three-Dimensional Framework Zirconium Phosphates, *J. Phys. Chem. C*, 2012, **116**(32), 17070–17081, DOI: 10.1021/jp304729s.

36 O. B. Lapina, D. F. Khabibulin and V. V. Terskikh, Multinuclear NMR study of silica fiberglass modified with zirconia, *Solid State Nucl. Magn. Reson.*, 2011, **39**(3–4), 47–57, DOI: 10.1016/j.ssnmr.2010.12.002.

37 A. J. Rossini, I. Hung, S. A. Johnson, C. Slebodnick, M. Mensch, P. A. Deck and R. W. Schurko, Solid-State ^{91}Zr NMR Spectroscopy Studies of Zirconocene Olefin Polymerization Catalyst Precursors, *J. Am. Chem. Soc.*, 2010, **132**(51), 18301–18317, DOI: 10.1021/ja107749b.

38 A. F. R. Kilpatrick, N. H. Rees, Z. R. Turner, J. C. Buffet and D. O'Hare, Physicochemical surface-structure studies of highly active zirconocene polymerisation catalysts on solid polymethylaluminoxane activating supports, *Mater. Chem. Front.*, 2020, **4**(11), 3226–3233, DOI: 10.1039/d0qm00482k.

39 P. He, B. E. G. Lucier, V. V. Terskikh, Q. Shi, J. X. Dong, Y. Y. Chu, A. M. Zheng, A. Sutrisno and Y. N. Huang, Spies Within Metal-Organic Frameworks: Investigating Metal Centers Using Solid-State NMR, *J. Phys. Chem. C*, 2014, **118**(41), 23728–23744, DOI: 10.1021/jp5063868.

40 C. Koschnick, R. Stäglich, T. Scholz, M. W. Terban, A. von Mankowski, G. Savasci, F. Binder, A. Schökel, M. Etter, J. Nuss, *et al.*, Understanding disorder and linker deficiency in porphyrinic zirconium-based metal–organic frameworks by resolving the Zr_8O_6 cluster conundrum in PCN-221, *Nat. Commun.*, 2021, **12**(1), DOI: 10.1038/s41467-021-23348-w.

41 G. Wissmann, A. Schaate, S. Lilienthal, I. Bremer, A. M. Schneider and P. Behrens, Modulated synthesis of Zr-fumarate MOF, *Microporous Mesoporous Mater.*, 2012, **152**, 64–70, DOI: 10.1016/j.micromeso.2011.12.010.

42 M. J. Katz, Z. J. Brown, Y. J. Colon, P. W. Siu, K. A. Scheidt, R. Q. Snurr, J. T. Hupp and O. K. Farha, A facile synthesis of UiO-66, UiO-67 and their derivatives, *Chem. Commun.*, 2013, **49**(82), 9449–9451, DOI: 10.1039/c3cc46105j.

43 A. Schaate, P. Roy, A. Godt, J. Lippke, F. Waltz, M. Wiebcke and P. Behrens, Modulated Synthesis of Zr-Based Metal-Organic Frameworks: From Nano to Single Crystals, *Chem. - Eur. J.*, 2011, **17**(24), 6643–6651, DOI: 10.1002/chem.201003211.

44 D. G. Cory and W. M. Ritchey, Suppression of Signals from the Probe in Bloch Decay Spectra, *J. Magn. Reson.*, 1988, **80**(1), 128–132, DOI: 10.1016/0022-2364(88)90064-9.

45 B. M. Fung, A. K. Khitrin and K. Ermolaev, An improved broadband decoupling sequence for liquid crystals and solids, *J. Magn. Reson.*, 2000, **142**(1), 97–101, DOI: 10.1006/jmre.1999.1896.

46 A. Bielecki and D. P. Burum, Temperature-Dependence of ^{207}Pb MAS Spectra of Solid Lead Nitrate - an Accurate, Sensitive Thermometer for Variable-Temperature MAS, *J. Magn. Reson., Ser. A*, 1995, **116**(2), 215–220, DOI: 10.1006/jmra.1995.0010.

47 R. S. Thakur, N. D. Kurur and P. K. Madhu, Swept-frequency two-pulse phase modulation for heteronuclear dipolar decoupling in solid-state NMR, *Chem. Phys. Lett.*, 2006, **426**(4–6), 459–463, DOI: 10.1016/j.cplett.2006.06.007.

48 R. K. Harris, E. D. Becker, S. M. C. De Menezes, R. Goodfellow and P. Granger NMR nomenclature - Nuclear spin properties and conventions for chemical shifts, *Handbook of Biochemistry and Molecular Biology*, 5th edn, 2018, pp. 903.

49 D. Massiot, F. Fayon, M. Capron, I. King, S. Le Calve, B. Alonso, J. O. Durand, B. Bujoli, Z. H. Gan and G. Hoatson, Modelling one- and two-dimensional solid-

state NMR spectra, *Magn. Reson. Chem.*, 2002, **40**(1), 70–76, DOI: 10.1002/mrc.984.

50 G. Kresse and J. Furthmuller, Efficient iterative schemes for ab initio total-energy calculations using a plane-wave basis set, *Phys. Rev. B: Condens. Matter Mater. Phys.*, 1996, **54**(16), 11169–11186, DOI: 10.1103/PhysRevB.54.11169.

51 J. P. Perdew, K. Burke and M. Ernzerhof, Generalized gradient approximation made simple, *Phys. Rev. Lett.*, 1996, **77**(18), 3865–3868, DOI: 10.1103/PhysRevLett.78.1396.

52 S. Grimme, J. Antony, S. Ehrlich and H. Krieg, A consistent and accurate ab initio parametrization of density functional dispersion correction (DFT-D) for the 94 elements H-Pu, *J. Chem. Phys.*, 2010, **132**(15), 154104, DOI: 10.1063/1.3382344.

53 P. E. Blöchl, Projector Augmented-Wave Method, *Phys. Rev. B*, 1994, **50**(24), 17953–17979, DOI: 10.1103/PhysRevB.50.17953.

54 G. Kresse and D. Joubert, From ultrasoft pseudopotentials to the projector augmented-wave method, *Phys. Rev. B: Condens. Matter Mater. Phys.*, 1999, **59**, 1758–1775, DOI: 10.1103/PhysRevB.59.1758.

55 M. Kaposi, M. Cokoja, C. Hutterer, S. Hauser, T. Kaposi, F. Klappenberger, A. Pöthig, J. Barth, W. Herrmann and F. Kühn, Immobilisation of a molecular epoxidation catalyst on UiO-66 and-67: the effect of pore size on catalyst activity and recycling, *Dalton Trans.*, 2015, **44**, 15976–15983, DOI: 10.1039/c5dt01340b.

56 P. Giannozzi, S. Baroni, N. Bonini, M. Calandra, R. Car, C. Cavazzoni, D. Ceresoli, G. L. Chiarotti, M. Cococcioni, I. Dabo, *et al.*, QUANTUM ESPRESSO: a modular and open-source software project for quantum simulations of materials, *J. Phys.: Condens.Matter*, 2009, **21**(39), 395502, DOI: 10.1088/0953-8984/21/39/395502.

57 N. Troullier and J. L. Martins, Efficient Pseudopotentials for Plane-Wave Calculations .2. Operators for Fast Iterative Diagonalization, *Phys. Rev. B: Condens. Matter Mater. Phys.*, 1991, **43**(11), 8861–8869, DOI: 10.1103/PhysRevB.43.8861.

58 L. Kleinman and D. M. Bylander, Efficacious form for model pseudopotentials, *Phys. Rev. Lett.*, 1982, **48**(20), 1425–1428, DOI: 10.1103/PhysRevLett.48.1425.

59 C. J. Pickard and F. Mauri, All-electron magnetic response with pseudopotentials: NMR chemical shifts, *Phys. Rev. B: Condens. Matter Mater. Phys.*, 2001, **63**(24), 245101–245113, DOI: 10.1103/PhysRevB.63.245101.

60 P. Pyykkö, Year-2017 nuclear quadrupole moments, *Mol. Phys.*, 2018, **116**(10), 1328–1338, DOI: 10.1080/00268976.2018.1426131.

61 J. B. DeCoste, G. W. Peterson, H. Jasuja, T. G. Glover, Y. G. Huang and K. S. Walton, Stability and degradation mechanisms of metal-organic frameworks containing the $Zr_6O_4(OH)_4$ secondary building unit, *J. Mater. Chem. A*, 2013, **1**(18), 5642–5650, DOI: 10.1039/c3ta10662d.

62 S. Devautour-Vinot, G. Maurin, C. Serre, P. Horcajada, D. P. da Cunha, V. Guillerm, E. D. Costa, F. Taulelle and C. Martineau, Structure and Dynamics of the Functionalized MOF Type UiO-66(Zr): NMR and Dielectric Relaxation Spectroscopies Coupled with DFT Calculations, *Chem. Mater.*, 2012, **24**(11), 2168–2177, DOI: 10.1021/cm300863c.

63 A. Nandy, A. C. Forse, V. J. Witherspoon and J. A. Reimer, NMR Spectroscopy Reveals Adsorbate Binding Sites in the Metal-Organic Framework UiO-66(Zr), *J. Phys. Chem. C*, 2018, **122**(15), 8295–8305, DOI: 10.1021/acs.jpcc.7b12628.

64 H. Eckert, J. P. Yesinowski, L. A. Silver and E. M. Stolper, Water in Silicate Glasses - Quantitation and Structural Studies by ^{1}H Solid Echo and MAS NMR Methods, *J. Phys. Chem.*, 1988, **92**(7), 2055–2064, DOI: 10.1021/j100318a070.

65 C. Gervais, C. Coelho, T. Azais, J. Maquet, G. Laurent, F. Pourpoint, C. Bonhomme, P. Florian, B. Alonso, G. Guerrero, *et al.*, First principles NMR calculations of phenylphosphinic acid $C_6H_5HPO(OH)$: Assignments, orientation of tensors by local field experiments and effect of molecular motion, *J. Magn. Reson.*, 2007, **187**, 131–140, DOI: 10.1016/j.jmr.2007.03.018.

66 A. E. Khudozhitkov, D. I. Kolokolov and A. G. Stepanov, Characterization of Fast Restricted Librations of Terephthalate Linkers in MOF UiO-66(Zr) by ^{2}H NMR Spin-Lattice Relaxation Analysis, *J. Phys. Chem. C*, 2018, **122**(24), 12956–12962, DOI: 10.1021/acs.jpcc.8b03701.

67 D. I. Kolokolov, A. G. Stepanov, V. Guillerm, C. Serre, B. Frick and H. Jobic, Probing the Dynamics of the Porous Zr Terephthalate UiO-66 Framework Using ^{2}H NMR and Neutron Scattering, *J. Phys. Chem. C*, 2012, **116**(22), 12131–12136, DOI: 10.1021/jp3029193.

68 J. d'Espinose de la Caillerie, C. Fretigny and D. Massiot, MAS NMR spectra of quadrupolar nuclei in disordered solids: The Czjzek model, *J. Magn. Reson.*, 2008, **192**, 244–251, DOI: 10.1016/j.jmr.2008.03.001.

69 S. Oien, D. Wragg, H. Reinsch, S. Svelle, S. Bordiga, C. Lamberti and K. P. Lillerud, Detailed Structure Analysis of Atomic Positions and Defects in Zirconium Metal-Organic Frameworks, *Cryst. Growth Des.*, 2014, **14**(11), 5370–5372, DOI: 10.1021/cg501386j.

70 I. Goodenough, V. S. D. Devulapalli, W. Xu, M. C. Boyanich, T.-Y. Luo, M. De Souza, M. Richard, N. L. Rosi and E. Borguet, Interplay between Intrinsic Thermal Stability and Expansion Properties of Functionalized UiO-67 Metal–Organic Frameworks, *Chem. Mater.*, 2021, **33**(3), 910–920, DOI: 10.1021/acs.chemmater.0c03889.